VIP *Very Important Paper*

Potential and Limitations of Research Battery Cell Types for Electrochemical Data Acquisition

Anna Smith,*[a] Pirmin Stüble,[a] Lea Leuthner,[a] Andreas Hofmann,[a] Fabian Jeschull,[a] and Liuda Mereacre[a]

Developing new electrode materials and/or electrolytes for lithium-ion batteries requires reliable electrochemical testing thereof. For this purpose, in academic research typically hand-made coin-type cells are assembled. Their advantage is a rather cheap and facile assembly, and possibility to prepare full-cells as well as half-cells, meaning cathode-anode or electrode-elemental lithium configurations. Critical parameters for testing data quality and the potential and limitations of cell tests in half-cell configuration are discussed. Further, on the basis of a round robin test, using highly homogenous commercial electrodes, where graphite is used as anode and $LiNi_{0.33}Mn_{0.33}Co_{0.33}O_2$ (NMC111) as the cathode material, it is shown that data acquired is highly influenced by assembling parameters. Besides known variables such as the amount of electrolyte or electrode positioning, the proper height of the cell stack and the steel grade of the housing material are identified as decisive variables. Finally, it is demonstrated that under proper conditions coin cells can show a great cycle stability of >2200 cycles using 1 C as dis-/charge rate while retaining a capacity of 80%. This performance is close to pouch-type cells containing the same electrodes and electrolyte, which were used as a benchmark system and showed >3500 cycles of lifetime.

Introduction

The electrification of society including electric vehicle and home storage applications, as well as consumer electronics is the major contributor to sustainable energy usage. State of the art electric energy storage systems are mainly based on lithium-ion battery (LIB) technology. However, the increasing demand of batteries to meet society's needs requires ongoing improvement of LIBs to further increase energy and power density. For the former, for instance, high energy materials like silicon based anodes[1] or high voltage cathode materials like $LiNi_{0.5}Mn_{1.5}O_4$ (LNMO)[2] are currently being investigated for their use in next generation LIBs. For the latter, commonly the cell itself is specifically designed, for example by use of thin electrodes, higher amounts of conductive carbons and/or nanotubes.[3] To investigate electrochemical performance, for example practical capacity determination, rate capability or long-term performance, these materials or novel electrode designs are typically tested on a pre-industrial level (R&D)

within coin-type cells or sometimes even in small pouch cells within research laboratories, where the results could be somewhat skewed if the cells do not meet high quality and reproducibility standards. Most industrial-type cells, which are fabricated in a highly automated manner on the other hand, very much meet these high quality standards.[4] However, it is impractical and costly to produce machine-made cells for research purpose where small quantities but a great flexibility of assembly parameters is needed. Therefore, it is vital to be aware of the potentials and limitations of coin-type cells. Coin-type cells can be assembled in so called "full-cell" or "half-cell" configuration, meaning an actual cathode-anode pair is used or only one electrode is investigated using lithium metal as the counter electrode, respectively. This is the major advantage of coin-type cells, as industrial type battery cells are always built in "full-cell" configuration and thus impede detailed investigations on the level of individual electrodes, for example capacity determination and redox pair studies. In fact, within the academic research community the most frequently build "cell-type" are half-cells rather than full-cells to validate the material development phase, where scale up and balancing electrode capacities are of no concern. This inevitably poses the questions, what conclusions can one draw from these coin cell experiments? How do the measured results translate into battery performance indicators of pilot scale materials and cell formats in full-cell configuration? In this context it is important to highlight that in a series of recent papers, bad practices in literature have been criticized more openly from different angles: Frith et al. attested tendencies in battery research to increasingly over-extrapolation of early lab scale findings as such cells are "free of several limitations that govern practical applications".[5] Johansson et al. chose a more humorous

[a] Dr. A. Smith, Dr. P. Stüble, Dr. L. Leuthner, Dr. A. Hofmann, Dr. F. Jeschull, L. Mereacre
Institute for Applied Materials (IAM)
Karlsruhe Institute of Technology (KIT)
Hermann-von-Helmholtz-Platz 1, 76344 Eggenstein-Leopoldshafen (Germany)
E-mail: anna.smith@kit.edu

Batteries & Supercaps

Research Article
doi.org/10.1002/batt.202300080

**Chemistry
Europe**
European Chemical
Societies Publishing

approach by listing the 'Ten Ways to Fool the Masses When Presenting Battery Research'.[6] Amine and coworkers summarized in their perspective "Bridging the academic and industrial metrics for next generation practical batteries" a number of crucial testing parameters that in their opinion are "often overlooked in academic literature but [that] are critical for practical applicability outside the laboratory".[7]

When comparing the "full-cell configuration" there are major differences from, for example pouch-type cell to coin-type cell: First of all, the electrolyte to active material ratio is much higher in coin cells and they are flooded with electrolyte (electrolyte volume to cell capacity ratio typically about 25–130 mL/Ah),[8,9] this study, which covers up decomposition and drying up of electrolyte resulting possibly in unrealistic good data. In sharp contrast, pouch-type cells have a much more realistic electrolyte amount to cell capacity ratio of <10 mL/ Ah.[10] Additionally, when considering a multi-layered electrode stack cell, there are thermal effects[3] that will never be observed in single-sided coated and single-layer stack coin-type cell configuration, nor as a single-layer stack pouch-bag cells. That is why for practical demonstration of performance one will always have to show electrochemical data in a multi-layered double-sided coated electrode configuration.

However, initially key performance indicators (KPIs) such as voltage curves, capacities, rate capability, and cycling stability of new materials for sake of costs and time have to be evaluated on smaller scale, which makes the coin cell a very suitable casing for academic research. Chen et al. highlighted key parameters in electrode preparation, the dimensioning of anode to cathode as well as areal capacity ratio of negative to positive electrode (N/P) and wetting time as most influencing in cell preparation to acquire best full-cell data.[11] Kowal et al. mainly investigated the influence of punching edge quality of the electrodes with respect to the electrochemical data obtained.[9] The Dahn group recently presented a guide for manufacturing hand-made coin cells, mainly focusing on the importance of electrode alignment in full-type coin cells.[12] The major issue of trying to produce benchmark data using coin-type cells, however, is the lack of information about best performance factors. When synthesizing new active materials and preparing self-made electrodes one might not know the "true" capability of material performance. In a similar study to this one by Bridgewater et al., self-made electrodes with measurable inhomogeneities and a rather low areal loading of 1 mAh/cm² were used to compare the electrochemical performances in different cell types: coin cell vs. single-layer pouch cell vs. multi-layer stacked pouch cell, mainly revealing that coin-type cells suffer from faster capacity decay with rather lower increase in resistance than pouch-type cells. On the other hand, multi-layer pouch cells suffered from greater resistance increase but lower capacity loss.[13] In a more recent publication by Dai and Cai best practice factors for coin vs. pouch cells are highlighted in theory with main focus on the electrode stack pressure.[14]

In this study we show the electrochemical performance of a single-sided coated single-layer electrode stack based on highly homogeneous commercial electrodes using LiNi$_{0.33}$Mn$_{0.33}$Co$_{0.33}$O$_2$ (NMC111) as the cathode and graphite as the anode active material in pouch-type configuration as a benchmark system for later comparison to coin-type full cell results. Using the same materials, we additionally show the performance difference of calendered vs. non-calendered double-sided coated single-layer electrode stack within a pouch cell, which is finally compared to a multi-layer pouch cell with a capacity of 8.85 Ah depicting application-relevant electrolyte volume to capacity ratio and thermal behavior. Further, the possibilities and limitations of coin cell tests in half-cell configuration are discussed and compared to corresponding full-cell coin cell test results. Initial data from full-cells using "established standard assembling procedures" were highly irreproducible and considerably worse than data obtained from pouch-type cells. Thus, a systematic round robin test involving scientist from four different groups and laboratories at the Institute for Applied Materials at Karlsruhe Institute of Technology (KIT) was carried out. Herein the findings as well as our suggestions for the best practice of coin cell manufacturing are reported on. For hand-made coin cells we show that major parameters influencing cell performance in assembly are a proper stack height and proper steel grade of the cell housing parts among known parameters like electrolyte amount and other above presented factors. In addition, some typically neglected but highly influential conditions on the testing data quality, such as proper cell connection and battery testing hardware are discussed.

Results and Discussion

The use of commercial, homogenous high quality electrodes[15] is absolutely necessary to show reproducible benchmark performance and guarantee that only cell building factors contribute to variances in electrochemical data. Therefore, commercial NMC111 as the cathode active material with an areal capacity of 1.75 mAh/cm² and graphite as the anode material with an areal capacity of 2.10 mAh/cm² (both measured @at 1 C in half-cells, see Figures S6 and S7), resulting in a N/P ratio of 1.2, were investigated in calendered (cal) state for single-sided coated (SS) electrodes, as well as in calendered (cal) vs. non-calendered (uncal) state for double-sided coated (DS) electrodes. The properties, such as areal mass loading, thickness and density of all electrode coatings are listed in Table 1. SEM images of the cross sections of electrodes are shown in Figure S1.

For the assembly of all cells care was taken to pair each cathode with an (in size) over dimensioned anode (using an overhang of 1 mm for coin-type and small laboratory pouch electrode stacks and 2 mm for large pouch cell electrode stacks around the edges). This guarantees that all cathode is covered by the anode area in case of misalignment of the electrode stack. Although this might result in some loss of lithium on overhanging graphite area by build-up of SEI, it prevents from lithium plating at the edges of the graphite electrode. On the other hand, it has also been reported that initial overhang

Batteries & Supercaps

Research Article
doi.org/10.1002/batt.202300080

Chemistry Europe
European Chemical
Societies Publishing

Table 1. General properties of the electrodes investigated. Cathodes: NMC111 on Al current collector (20 μm thickness), anodes: graphite on Cu current collector (10 μm thickness). The loading refers to one electrode side (active materials, conductive additives and binder). The (single side) electrode layer thicknesses were derived from the corresponding SEM images that are shown in Figure S1.

Electrode	Coating	Calendering	Loading [mg/cm^2]	Thickness [μm]	Density [g/cm^3]	Label in image (Figure S1)
Cathode	Double-sided	Uncalendered	13.9(2)	67(2)	2.1	DS-uncal (a)
Cathode	Double-sided	Calendered	13.7(2)	52(2)	2.6	DS-cal (b)
Cathode	Single-sided	Calendered	13.9(2)	55(2)	2.5	SS-cal (c)
Anode	Double-sided	Uncalendered	7.7(2)	68(2)	1.1	DS-uncal (d)
Anode	Double-sided	Calendered	7.5(2)	49(2)	1.5	DS-cal (e)
Anode	Single-sided	Calendered	7.4(2)	57(2)	1.3	SS-cal (f)

lithium loss can result in a lithium sink/reservoir that can become available at slower C-rates.[16]

Benchmark pouch-type cells – rate performance and effect of calendering

Images of KIT-BATEC small laboratory pouch cell (LPC) and the multi-layered stack 9 Ah pouch cell (9 Ah), are shown in Figure 1(a) and (b), respectively. Within this study these pouch cells function as a reference system to assess the coin cell performance. Incorporating the above described electrodes single-layer stack LPCs result in a nominal cell capacity of 43 mAh, while multi-layer stack 9 Ah cells containing nine cathodes result in 8.85 Ah.

As listed in Table 2, cathodes and anodes in calendered and non-calendered state were built in the four possible pairings as

double-sided coated electrode in a single stack (one cathode and one anode separated by one layer of separator) into small pouch-type cells (LPC-1 to LPC-4). For comparison also single-sided-coated calendered electrode pairs were assembled into cells (LPC-5). All configurations were built and tested in triplicate. After formation, all cells underwent an asymmetric rate test in discharge direction, see Figure 2, for a plot of relative capacities (and S2 for absolute capacities) vs. C-rate.
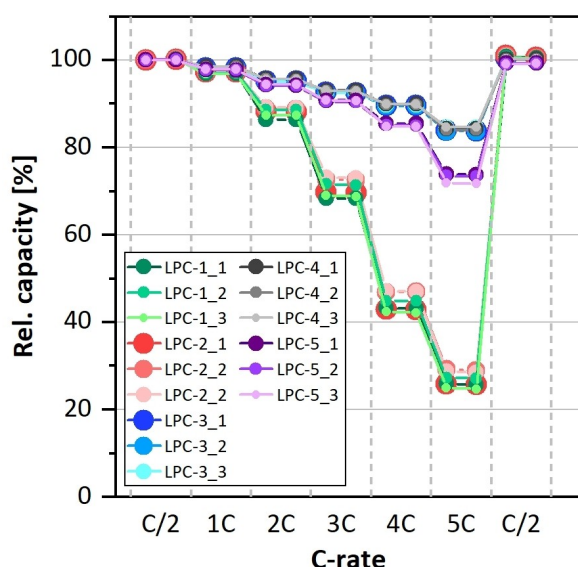
The test was performed with a constant charge condition, namely C/2 until reaching a potential of 4.2 V, followed by CV-phase until $I < C/20$. On the discharge sequence the current was varied from C/2, over 1 C, 2 C, 3 C, 4 C, 5 C and back to C/2 to check for degradation effects due to high current discharge. Each rate cycle was performed twice. In general, LPCs made of double-sided coated electrodes (LPC-1–LPC-4) show a starting capacity (after formation) at C/10 of ~45 mAh, while the single-sided coated electrode based cells (LPC-5) have a capacity of
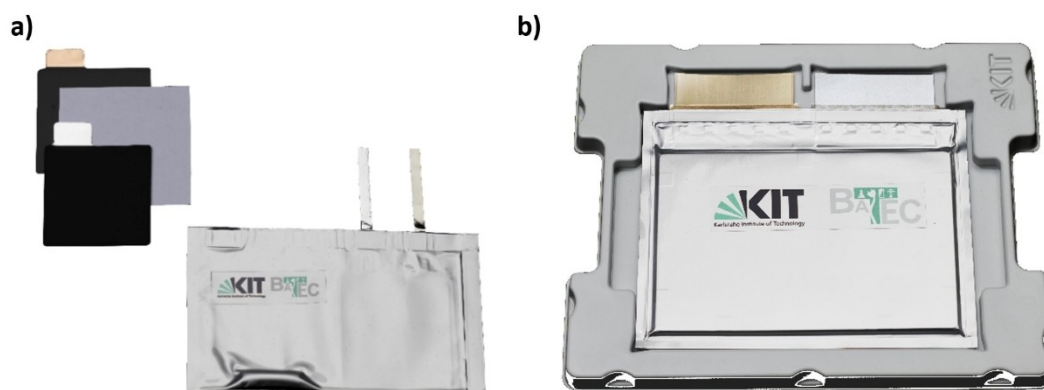
Figure 1. a) Photo of a KIT-BATEC laboratory pouch cell (LPC) including cell components with a cathode foot print of 5×5 cm (LPC-1–LPC-5). b) KIT-BATEC multi-layer large format pouch cell with a cathode foot print of 13.5 cm×20.8 cm (9 Ah).

Table 2. Overview of the different pouch cells investigated in this study. More detailed information on the properties and building conditions are given in the Experimental Section.

Pouch format	Laboratory pouch cell (LPC)					Large pouch cell
Label	LPC-1	LPC-2	LPC-3	LPC-4	LPC-5	9 Ah
Footprint [cm^2]			~5×5			~14×21
Cathode	DS-uncal	DS-uncal	DS-cal	DS-cal	SS-cal	9×DS-cal
Separator			CC-PET			
Anode	DS-cal	DS-uncal	DS-cal	DS-uncal	SS-cal	10×DS-cal
Electrolyte			1 M LiPF$_6$ in EC/DMC + 3 wt.% VC			
Volume [mL]			0.7		0.45	35
Vol/cap [mL/Ah]			16		10	4

Batteries & Supercaps

Research Article
doi.org/10.1002/batt.202300080

Chemistry
Europe
European Chemical
Societies Publishing

Figure 2. Asymmetric rate performance test in discharge direction with constant charge of C/2 and discharge varied from C/2 to 5 C on laboratory pouch cells (LPC) containing single/double-sided, non/calendered electrodes, see Table 2 for composition of cell build up. Plot shows triplicated data (_1–_3) for realative capacities vs. the C-rate.

43 mAh, (see S2). This is very likely due to some interference of the inactive cathode side, where lithium ions got deintercalated and are available for active capacity contribution. Comparing the cells build from double-sided coated electrodes (*LPC-1–LPC-4*) to one another, one can observe a high capacity retention of 85% at 5 C for cells composed of calendered electrode pairs (*LPC-3*), as well as for cells including the pair of calendered cathode/ uncalendered anode (*LPC-4*). On the other hand, the cells that are build from pairs uncalendered cathode/calendered anode (*LPC-1*) and uncalendered cathode/ uncalendered anode (*LPC-2*) only deliver <30% of their initial capacity at 5 C. The deviation in performance already starts at a rate of 2 C. This outcome emphasizes on the importance of densification of the NMC-based cathode consisting of poor electrically conducting NMC particles.[17] Pressing of the cathode results in an efficient electrically conducting network throughout the particle matrix (conductive carbon and NMC particles), but also improves the interface resistance of the coating/ current collector with increase in overall electric conductivity,[18] wheras there is essentially no adverse effect on the cells' rate capability when densified graphite anodes are used. Comparing single-sided to double-sided coated calendered electrode pairs a difference in performance was noted, namely that the single-sided coated electrodes in *LPC-5* had a lower rate capability (~72% at 5 C) than double-sided coated electrodes in *LPC-3* (~85% at 5 C). This might be explained by slightly lower electrode density in *LPC-5* vs. *LPC-3*, resulting from different compression (cf. Table 1). All cells show their respective initial capacities in the final C/2 check rate, meaning that neither cell type degraded upon rate testing in discharge direction.

The data shown here emphasize on the importance of proper densification of electrodes, which enables optimal particle-particle distances, for example active material to conductive material or current collector, and decreasing the overall resistances of the electrode. While pressing of electrodes is important for these obvious reasons, there is always an optimal degree of densification and with that the porosity of the electrodes. In contrast, too severe pressing/calendering will have negative effects such as particle cracking, perforation of the current collector by particles or simply too low amount of porosity for ideal wetting with the electrolyte.[19] In summary, performing rate tests, possibly starting as low as 1 C depending on the overall active mass loading of the electrode, could be meaningless when using electrodes with improper densification.

Benchmark pouch-type cells – long term cycling

Long term performance studies were conducted for single-layer lab-size pouch-type cells based on either double-sided (calendered vs. non-calendered) or single-sided coated calendered electrodes (*LPC-1–LPC-4* vs. *LPC-5*, respectively), and multi-layer stack large pouch cells (*9 Ah*, see Figure 1b) based on double-sided coated calendered electrodes (see also Table 2 for information on composition of cells). The cells were cycled with a CCCV 1 C–CC 1 C charge-discharge protocol and data (mean values from three individual cells together with error bars from standard deviation) is shown in Figure 3 for a) relative capacity, b) areal capacity based on cathode size and c) areal inner resistances measured for SOC 30% (see Figure S3 for complete set SOC 10, 30, 50, 70 and 90%), over nearly 4000 cycles.

All pouch cells containing calendered electrodes (*LPC-3*, *LPC-5*, *9 Ah*) show a stable and very reproducible long-term performance over multiple thousands of cycles with a nearly linear capacity fade up to ~3500 cycles (note *LPC-3* have only reached 1600 cycles thus far) until a remaining capacity of 80% is reached, see Figure 3(a) for relative capacity decay. The coulombic efficiency (CE) is above 99.8% for the first 2500 cycles showing no indications of charge loss (see Figure S4). Looking at the pouch cells containing the non-calendered electrode pair (*LPC-2*), one can see a much greater decay of capacity starting after a few hundred cycles. Also, the cells containing non-calendered cathode but calendered anode (*LPC-1*) show similar capacity decay to *LPC-2* however with slightly lower slope in decay. In contrast, *LPC-4*, which is composed of calendered cathode and non-calendered anode shows initial relative capacity decay comparable to *LPC-3* with sudden increase in decay at 700 cycles. Overall, the cell capacity decay is affected more negatively by incorporation of non-calendered anodes than non-calendered cathodes within long-term tests applying 1 C cycling rate. A possible reason could be greater lithium plating or SEI growth at the graphite particles within non-calendered electrodes (due to inhomogeneities in electrode thickness/ electric conductivity). When comparing absolute capacity fade in terms of areal cathode capacity decay, one can observe that the *9 Ah* multi-layered stack cell provides greater (~3%) overall absolute capacities than single-sided coated electrodes from *LPC-5* (see Figure 3b). In direct comparison, double-sided coated electrodes independent of their
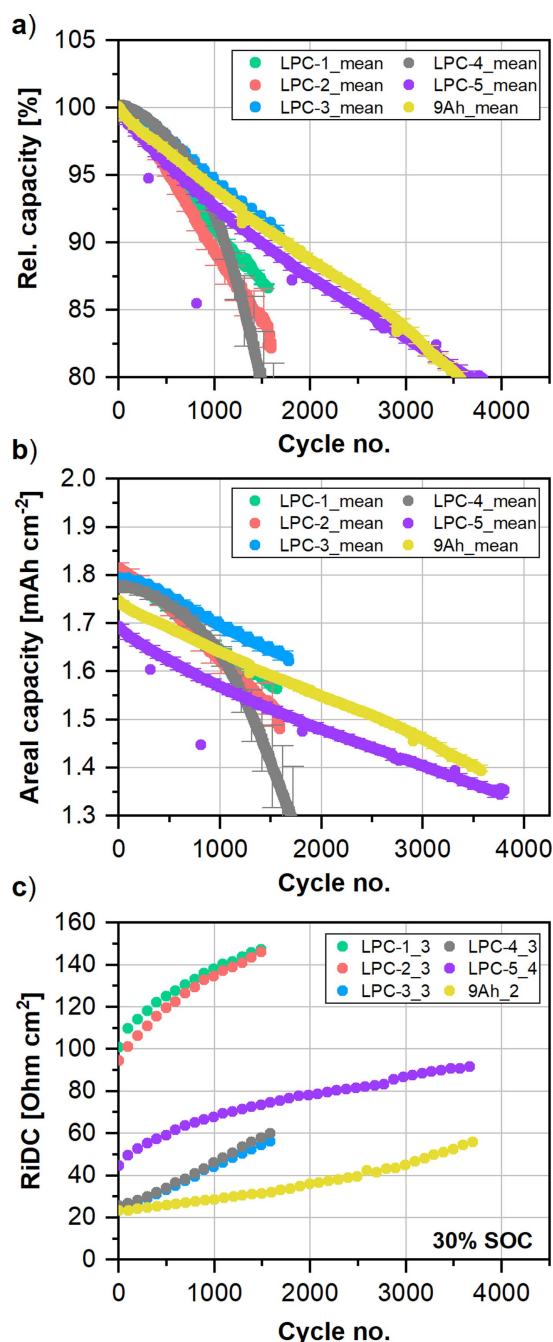
Figure 3. a) Long-term performance data of KIT-BATEC pouch-type cells using 1 C for charge and discharge showing the relative capacity decay of different electrode pair containing laboratory pouch cells (LPC-1—5: various non/calendered pairs) and multi-layered type cells (9 Ah) over the number of cycles. b) same data as (a) but capacity is normalized to cathode area for absolute capacity decay comparison of different cell sizes. Figure (a and b) depicts mean values together with error bars from standard deviation of three individual cells each. c) Representative areal inner direct current resistances at SOC30 vs. cycle number for cells from Figure (a and b).

compression state deliver higher absolute capacities in single-layer stack (LPC-1—LPC-4) (initially) as in multi-layer stack configuration. Most likely extra capacity/lithium ions are delivered from the outward-facing cathode-side in LPC1—LPC-4. It should be noted that in this study, the multi-layer electrode

stack 9 Ah cell did not generate significant heat during cycling (cell temperature was monitored on the surface with average of 28 °C). This can very much differ using for example other type of electrode material/ composition, or higher areal loadings of the electrodes, thus causing greater thermal effects during charge and discharge. A direct projection of cyclic ageing data in such case from single-layer to multi-layer cell will differ as single-layer stack electrode cells will never cause substantial heat evolution resulting in different thermal ageing effect than multi-layer stack pouch cells. Typically, in large format cells the change of inner resistance (RiDC) is monitored and used to qualitatively compare ageing for same cell types under different conditions. Using Ohm's law RiDC values are calculated from a defined pulse length at given SOC. Here, the RiDCs at SOC 30 % (measurements were taken every 100 cycles) are normalized to the total active cathode area for the given pouch cells and displayed in Figure 3(c) (see Figure S3 for complete RiDC data sets). The results show that a comparison between different cell types is challenging on the basis of such RiDC measurements. However, a direct comparison can be made between single-stack electrode containing pouch cells built from double-sided coated electrodes. As indicated from the rate test, see section above, similar RiDC values are found for LPC-1 and LPC-3, where compression of the cathode has a great effect on overall cell resistance. One can find a four-fold higher inner resistance of the cells containing non-calendered cathodes (independent of compression state of the anode) compared to cells containing calendered cathodes (independent of the compression state of the anode). Overall, the slope for RiDC value over cycle number is similar for LPC-1—LPC-4. Also, the slope increase of the RiDC vs. cycle number is greater for LPC-1—LPC-4 than for LPC-5 and 9 Ah cell. The change in RiDC over cycle number of the 9 Ah cell (double-sided coated electrodes) is comparable to LPC-5 (single-sided coated electrodes), where all cathode material in the cell is active. However, for LPC-5 one can find a steeper increase in the beginning, whereas for the 9 Ah cell the RiDC increases stronger over time.

In addition, the voltage response within the 20 s 1 C pulse is displayed in Figure S5 for all cells, where an RiDC test was performed. A detailed investigation on the interpretation of the RiDC data is certainly rather inappropriate keeping in mind that just a simple change in voltage after 20 s caused by a 1 C pulse was used here, where individual cell processes (e.g., ohmic resistance, charge transfer, diffusion) cannot be resolved from another. More detailed experiments, for example time resolved analysis of the voltage change within pulsing,[20] or even impedance analysis are beyond the scope of this work. However, since the change in voltage over time after the first drop is essentially the same for all cells, see Figure S5, one can analyze and compare the ohmic resistance for all cells. Overall, the pouch cell 9 Ah has the lowest internal resistance, followed closely by LPC-3/LPC-4, and then by some distance LPC-5. The highest drop in voltage and with that highest resistance was obtained for LPC-1/LPC-2.

Reproducibility of coin-type cells

As demonstrated in the first part of this work, it is possible to produce pouch cells with state-of-the-art electrode materials in single-layer as well as multi-layer electrode stack configuration on a pilot scale with high reproducibility and comparable long cycle life. However, most laboratories rarely use pilot scale equipment, do not work with optimized electrode formulations from an industrial coater, nor is it common that lab scale electrodes are uniformly calendered. For battery research laboratories, working mostly in the domain of material development, this does not have to be a shortcoming by any means, as long as the limitations of cycling results in half- and full-cell configurations in a small laboratory scale environment, for example on the basis of Swagelok or coin-type cells, are clearly communicated and discussed within the framework of material characterization.

The incentive with the following sections is to critically review the cell components that are commonly used, as well as assembling habits that are practiced/even taken for granted in laboratory work. As will be demonstrated it is those components that influence reproducibility and quality of lab results.

The first section will investigate on a comparison between half- and full-cell results, following the "standard assembly procedure" established in one of our material research laboratories. From there, we will discuss the results of a round robin test within our different battery labs, where we discuss the impact of different (inactive) cell components and test equipment on typical KPIs, such as capacity retention and rate capability. For comparability with the above presented pouch cell results (*LPC-5*), the same materials (NCM111&graphite based single-sided coated calendered electrodes) and the same electrolyte formulation were used.

Comparing half- and full-cell configurations

Experiments presented in this section refer to results from a single lab (*CC-type_E, _F, _G*) with the aim to work out performance differences of half- and full-cell configurations. A summary of the cell characteristics of the investigated half- and full-cells is provided in Table 3. Because of the use of Li-foil (250 μm) half-cell stacks exhibited generally a higher stack size as compared to full-cells. For the latter an anode capacity over-balancing of about 10% was employed (N/P = 1.1 @C/10). In the following the different electrochemical behaviors during formation, rate-capability and long-term cycling stability are discussed.

Formation cycles: potential curves and initial capacities

In Figure 4(a), the discharge capacities (mean values from five individual cells together with error bars from standard deviation; defined as delithiation of graphite and lithiation of NMC according to a full-cell configuration) for four formation cycles at C/10 are shown for the half-cells *CC-type_F* (graphite vs. Li),

Table 3. Cell composition for tested half-cell stacks and the corresponding full-cell configuration using a CR2032 coin cell. Note that stack heights including spring height and internal can height will be discussed in a later section.

Format	Coin cell (CR2032), half- vs. full-cell config.		
Label	*CC-type_F*	*CC-type_G*	*CC-type_E*
Cathode or Li	Li	SS-cal	
Separator	GF/B		
Anode or Li	SS-cal	Li	SS-cal
Electrolyte	1 M LiPF$_6$ in EC/DMC + 3 wt.% VC		
[μL]	350		
Thickness of the individual components [mm]			
Metal spacer	0.500	0.500	0.500
Cathode or Li	0.250	0.055	0.055
Separator	0.600	0.600	0.600
Anode or Li	0.057	0.250	0.057
Stack height	**1.407**	**1.405**	**1.212**
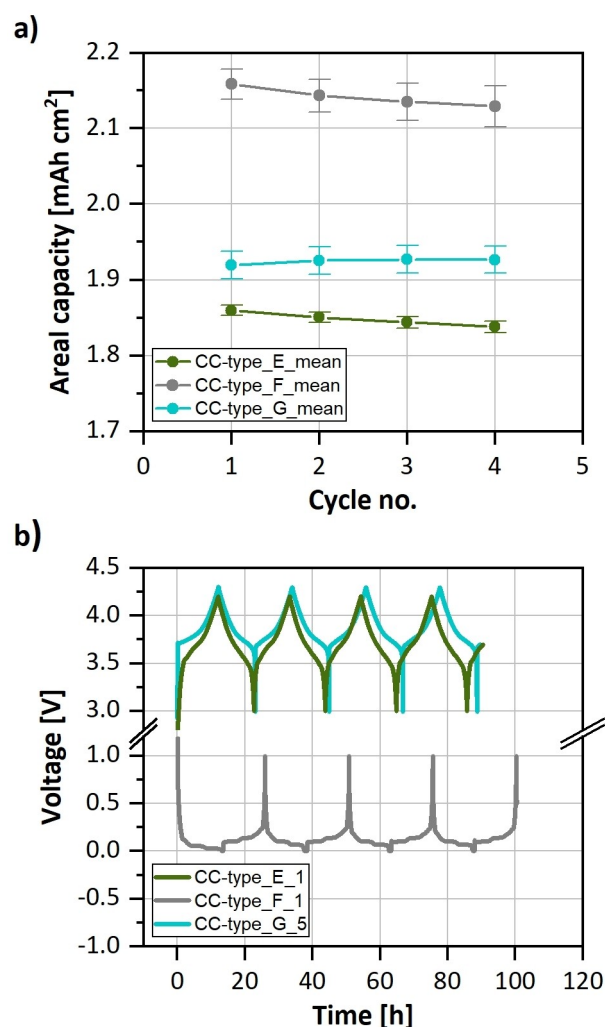
Figure 4. a) Areal half-cell vs. full-cell formation capacities based on mean values together with error bars from standard deviation of five individual cells each. b) Potential curves for NMC111 and graphite vs. Li from half-cells (graphite: CC-type_F; NMC111: CC-type_G) compared to the full-cell (CC-type_E) voltage profile during formation.

CC-type_G (NCM111 vs. Li) and the full-cell configuration *CC-type_E* (NCM111 vs. graphite). The corresponding voltage

profiles are shown in Figure 4(b). As mentioned above the negative electrode has a higher areal capacity than the cathode, thus *CC-type_F* shows about 10% higher capacity @C/10 than *CC-type_G*. It is also observed that the full-cells show slightly lower capacities than the cathode half-cell, which is a result of a limited lithium inventory in full-cells that is partly consumed irreversibly on the graphite surface during SEI formation. In addition, full cells display a small capacity decay over the first four cycles as a consequence of recurrent irreversible reactions, whereas cathode half-cells maintain their capacity over the same duration and even gain some capacity from the first to the second cycle. The behavior of the latter was attributed to the fact that any lost Li will be replenished by the vast excess of metallic lithium at the counter electrode so that despite Li losses all available Li sites in the cathode active material will be filled on consecutive cycles. On the other hand, graphite half-cells show some initial capacity loss, which can be attributed to SEI formation and possibly some material degradation in the process until a protective layer has fully formed.

To demonstrate that the electrodes perform as expected, the individual voltage profiles for active materials tested in the half-cell configurations are shown in Figure 4(b) and compared with that of the full-cell configuration. Graphite shows two characteristic staging processes with distinct plateaus, while NCM111 displays a sloping profile that starts out with a small slope that becomes steeper in the second half of the oxidation process towards the upper cut-off potential. The differences in areal capacity of anode and cathode is also reflected in slightly longer charge/discharge sequences of the graphite anode, as the applied areal current (and with that C-rate) for both cases was the same. Theoretically, the full-cell profile is the difference between the two half-cell profiles. In Figure 4(b), the experimentally obtained profile is shown. Because of the capacity loss in the full-cell configuration the cycling sequences become shorter with cycle number. To analyze the origins of the capacity fade in more detail, three-electrode measurement setups would be required. However, such experiments are best conducted in dedicated cell geometries/parts, with a reference electrode, as well as advanced cycling equipment with a separate reference sense. One possibility using a coin-cell setup is for instance incorporation of a thin lithiated PTFE coated Au wire.[21]

Rate capability and long-term performance

After the formation of full- and corresponding half-cells (see section above) the same rate test as already described at the beginning of the results was performed on all cells. The rate dependent step was for all cells in direction of delithiation of graphite/ lithiation of cathode material, corresponding to discharge direction of the full-cell. From the data shown in Figure 5(a) one can see that the graphite anode has almost no capacity decay up to 3 C, and only 25% capacity fade at 5 C delithiation rate. On the other hand, the rate stability of the NMC111 electrode is highly impacted starting already at C/2, with capacity loss of ~35% at 5 C (note that these half-cells had a capacity of >1.9 mAh/cm^2 at C/10 in Figure 4(a) and 1.8 mAh/ cm^2 at C/2, see Figure S6). These findings might not be surprising due to the much greater electronic conductivity of graphite over cathode active materials like NMC111. Interestingly, the corresponding full-cells show even lower rate performance, suggesting that the rate capability of the full cell is – somewhat counterintuitively - not limited solely by the slower electrode. This is also interesting from the perspective of impeding surface layer thicknesses. The SEI is believed to be the impeding factor for high rate-capability of graphite electrodes, for example when compared to LTO.[22] Furthermore, the SEI in half-cells is typically thicker than in a full-cell, which has been shown for example in photoelectron spectroscopy studies.[23–25] This finding can be ascribed amongst other factors to the deep lithiation on every cycle due to the vast excess in Li inventory (full cells with a N/P graphite excess and a limited Li inventory do not reach the fully lithiated graphite stage). Moreover, in the 2-electrode setups, the resistance of the Li
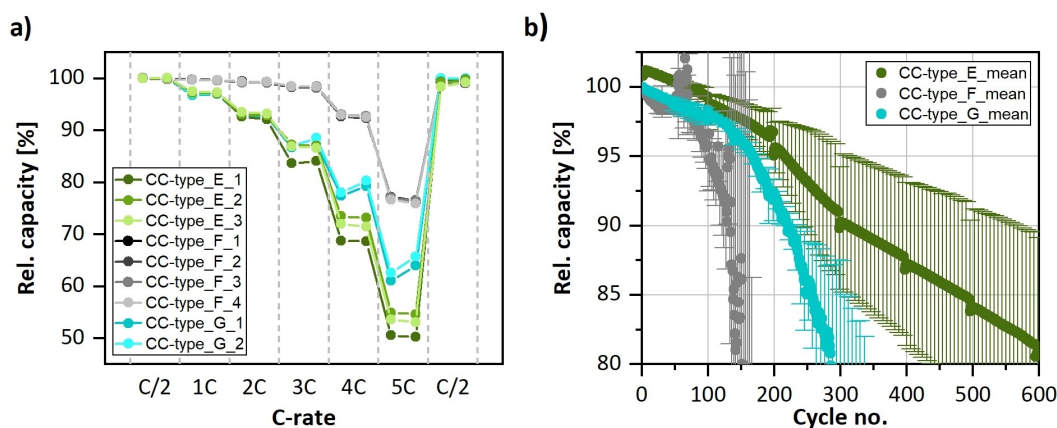
Figure 5. a) Rate capability and b) long-term performance using 1 C dis/charge rate of half-cells [CC-type_F (grey): Li vs. graphite; CC-type_G (cyan): NCM111 vs. Li] compared to corresponding full-cell [CC-type_E (green): NCM111 vs. graphite]. b) depicts mean values together with error bars from standard deviation of five individual cells each.

Batteries & Supercaps

Research Article
doi.org/10.1002/batt.202300080

Chemistry Europe
European Chemical
Societies Publishing

electrode must not be neglected. Depending on the current density lithium metal plating/ stripping has kinetic limits. Over only a few cycles, like in the rate-test, this effect may not play a decisive role but generally, its interfacial resistance can make a significant contribution to the rate performance.[26] Another important difference could be the cell stack height and thus the stack pressure due to intrinsically thicker Li foil in half cells (CC-type_F, _G) compared to full-cells (CC-type_E), see Table 3, causing different cell resistances and with that pre-mature voltage cutoffs.

For another set of cells long-term cycling at a constant charge-discharge rate of 1 C was performed after the formation cycles. The relative areal capacity decay (mean values from five individual cells together with error bars from standard deviation) is displayed in Figure 5(b). It can be readily seen that the life time of half-cell setups is inferior to the long-term stability of full-cell configurations. In addition, it is seen that the graphite half-cell (CC_type_F) fades faster than the NCM111 half-cell (CC_type_G). The comparison is a nice example, how different degrees of irreversible reactions affect the cycle life of half-cells despite the vast lithium excess that was initially built into the coin cell using the metallic lithium counter electrode. The faster fading of the graphite electrode is attribtued to several detrimental effects. Firstly, the areal capacity is higher than for the cathode (balancing difference at 1 C is ~20% higher capacity, see also Figure S7). Although the cells were cycled with the same C-rate, more lithium is stripped and plated from the counter electrode each cycle due to the active material excess in the anode. The final rapid capacity decay that is seen for graphite electrodes after around 100 cycles, for NCM111 after about 150 cycles, is likely initiated by lithium dendrite growth leading to possible micro-shorts (see as fluctuating capacities, especially for the graphite half-cell) and because of accelerated electrolyte consumption due to recurrent exposure of freshly deposited lithium. It is well-known that the surface layers on the cathode side are much thinner, thus suggesting that less side reactions occur at this electrode. This is partly reflected in the longer cycle life of the cathode half-cell. Moreover, previous studies demonstrated that the cycle life of half-cells strongly scales with electrolyte amount.[11] In contrast, full-cells initially perform similar to the cathode half-cells and show significantly slower fading until a relative capacity of 80% is reached for reasons discussed above. What's striking, however, is the high spread of the cell performance in the presented cells. This is especially pronounced for full-cells (CC-type_E) in this test, as they cycled the longest and reproducibility between cells of the same type decreased considerably with increasing cycle number.

To summarize, monitoring of the respective half-cell potentials are indispensable in material development, as they allow to study material specific electrochemical characteristics, for example potential plateaus indicating phase changes, and therefore provide detailed insight into the individual electrode processes. However, when discussing long-term performance on the basis of half-cell data it is worth considering a couple of influencing factors that may well limit the extend of life time predictions on this level.

Cross talk phenomena can have significant impact on long-term capacity retention. In half-cells cross talk is routed in side reactions with the reactive lithium interface caused by the repeating stripping/plating processes. Therefore, electrolyte (additive) consumption[27] and accumulation of degradation products can be quite severe. In cathode half-cells, but with greater impact in full-cells, cross talk may also result from transition metal leaching.[28]

Half-cell configurations exhibit essentially an infinite lithium reservoir at the counter electrode, while full-cells show a limited lithium inventory. However, cycling lithium over hundreds of cycles leads to severe wear-out with build-up of additional cell resistance and eventually failure modes through dendritic lithium that restricts the long-term use of metallic lithium counter electrodes. More importantly, aging and wear-out of the lithium electrode is a function of current density, i.e., the amount of Li that is plated and stripped during each cycle. Working electrodes with low areal loadings may last significantly longer than the electrodes with the same electrode material but higher areal loading. Cycle life thus becomes dependent on electrode loadings, lithium thickness (excess) and applied current density/C-rate.

Round Robin test – coin-cell configurations

Given the large spread we observed in the full-cell data in Figure 5(b) the question arose how the cell performance can be further optimized. Therefore, cell assembly and tests were expanded to different labs within a round robin study in order to identify the most relevant external parameters for poor cell performance and/or reproducibility. Electrode materials and the electrolyte were provided, but each lab was free in chosing separator and electrolyte amount, as well as assembling procedure. The cycling procedure was the same for all samples. Furthermore, we focused on full-cell results to be able to compare the data with the obtained pouch cell results above. As can be seen in Table 4 the procedures and some of the materials (seperator, coin cell parts) differ between labs.

Besides the CC-PET ceramic separator, a variety of alternative and commonly used separator materials were investigated. The separator also influences the stack height and thus the cell pressure, which will be discussed in a later section. It can also be seen that different labs used different electrolyte volumes. A factor discussed less frequently is the type of coin-cell steel, which we discuss in the following section. Lastly, it is worth mentioning that across our labs different cycling equipment and cell rigs were installed, which have a different impact on the obtained test results, see below. Differences in the cycling conditions further extend to the operation temperatures, which was controlled either in a climate chamber or by AC room cooling. These structures are historically grown and are often difficult (and expensive) to change. Therefore, it is even more important to be aware of potential sources of error stemming from infrastructure.

The results of this round robin experiment are shown in Figure 6 that visualizes the practical data outcome for long-

Batteries & Supercaps

Research Article
doi.org/10.1002/batt.202300080

Chemistry Europe
European Chemical
Societies Publishing

Table 4. Cell composition for tested cell stacks in a CR2032 coin cell with an available stack space of 1.05 to 2.4 mm.

Format	Coin cell (CR2032), full-cell configuration				
Label	CC-type_A CC-type_A2[a]	CC-type_B	CC-type_C CC-type_C2[b]	CC-type_D	CC-type_E[b] CC-type_E2[a,b]
Cathode	Single side coated, calendered				
Ø [mm]	14	14	14 (C)/15 (C2)	14	14
Separator	GF/C	CC-PET	QM-A	CC-PET	GF/B
Anode	Single side coated, calendered				
Ø [mm]	16	16	16	16	16
Electrolyte	1 M LiPF$_6$ in EC /DMC + 3 wt.% VC				
[μL]	200	350	110	350	350
[mL/Ah]	74	130	40	130	130
Thickness of the individual components [mm]					
Metal spacer	1.000	1.000	1.000	0.500	0.500
Cathode	0.055	0.055	0.055	0.055	0.055
Separator	0.260	0.035	0.475	0.035	0.600
Anode	0.057	0.057	0.057	0.057	0.057
Stack height	**1.372**	**1.147**	**1.587**	**0.647**	**1.212**
Comment	Steel type and testing rig variation		Best practice, CC-type_C2 with RiDC	failed	Steel type variation, RiDC

If not indicated otherwise, all cells are made from SUS316L steel ([a]SUS304), [b]RiDC measurements were included within cycling test. For CC-type_A and _A2, each 10 cells were built, for CC-type_B to _E2 at least 5 cells were tested. Rate capability tests were performed with CC-type_C2, _E and _E2. CC-type_E has already been listed in Table 3. It is mentioned again to increase comparability.

a)

b)
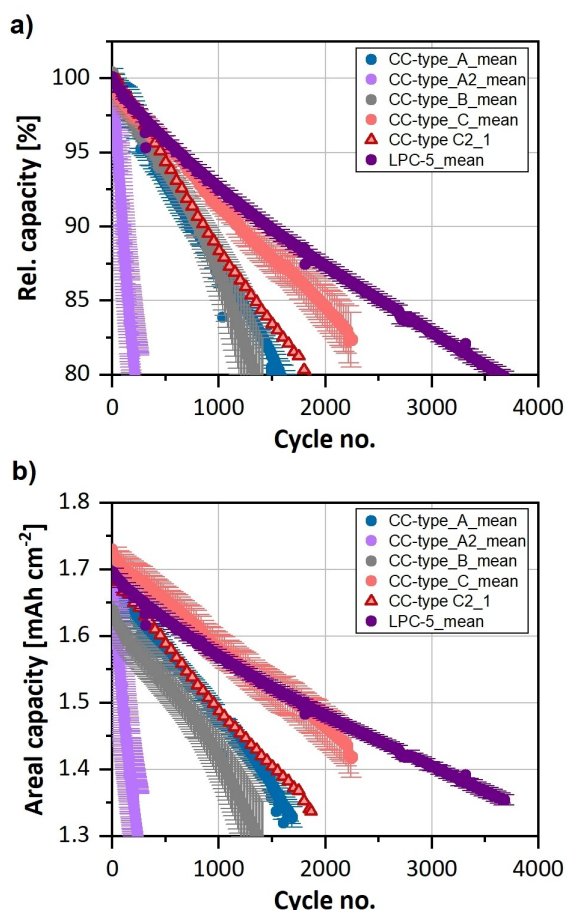
Figure 6. Long-term capacity decay: a) relative decay; b) absolute decay (per cm^2 cathode) upon 1 C charge/ discharge vs. cycle number for coin cells that were assembled considering proper conditions in comparison to the benchmark pouch cells. Mean values and error bars from standard deviation were determined from five (CC-type_A, _A2, _B, _C) and four (LPC-5) individual cells each.

term testing using the 1 C charge and discharge cycling protocol used in the previous sections. Data from the formation cycles will be discussed in a different context in a later section. In addition to the coin-cell data, Figure 6, also provides benchmark data of laboratory pouch cells (LPC-5) that are based on the same single-sided coated calendered electrode sheets. A plot of the relative capacity decay and absolute capacity decay normalized to the area of the cathode used within the cell (mAh/cm^2 cathode) is provided in Figure 6 a and b, respectively (mean values from five [CC-type_A, _A2, _B, _C] and four [LPC-5] individual cells together with error bars from standard deviation as well as data of one CC-type_C2 cell).

Compared to the LPC-5 cells, all coin-cells show lower absolute capacities based on cathode area and faster capacity decay, except for CC-type_C showing initially higher areal capacities. Note that pouch cells had an embedded a RiDC measurement every 100 cycles, while coin cells were tested continuously for the sake of time, with exception of CC-type_ C2. The samples CC-type_D are not shown in Figure 6, since all cells failed with great irreproducibility (see Figure S8 for fluctuating voltage profile of formation data). The failure was due to the small stack height that was deliberately minimized by using a thin CC-PET separator and a thinner coin cell spacer. CC-type_C samples showed a capacity retention that was comparable over most part of their cycle life with that of LPC-5 cells, but with a larger standard deviation. Significantly faster but similar capacity decay was observed for samples CC-type_A, CC-type_B and CC-type_C2 (only one sample shown, rate test was performed before the long-term test which included a RiDC test and a larger cathode, namely 15 mm in diameter). The poorest performance was obtained from CC-type_A2. The differences between samples CC-type_A and CC-type_A2, as well as CC-type_E and CC-type_E2 are the coin cell part materials. Coin cells made from SUS316L steel performed considerably better. Another major difference between the

Batteries & Supercaps

Research Article
doi.org/10.1002/batt.202300080

Chemistry Europe
European Chemical
Societies Publishing

samples are the stack heights (lower for *CC-type_A* and *CC-type_B* than for *CC-type_C*), which is a result of the different separators used. Higher stack height also implies higher stack pressure, which could lower the cell resistance, and with that result in higher measured capacities. The separator material is a factor in itself that should deserve more attention, as the separators' compressibility, tortuosity, chemical inertness and wetting properties could also play a crucial role for both stack pressure and long-term performance. For instance, examples how dendrite growth proceeds differently through separator layers can be found in the literature.[29] A way to extend the lifetime of half-cells is to use a separator stack which has a PE/PP separator layer included. This surpresses the dendrite growth through the separator as demonstrated by Mereacre et al.[30] Moreover, a parameter associated to the choice of separator is the electrolyte volume, since many glass fiber-based separators require larger amounts of electrolyte to be fully soaked. Furthermore, glass fiber separators have no practical relevance on industrial cell level and are used exclusively on a lab scale. The separators chemical compatibility will be discussed in the section "Other Considerations for Cell Manufacturing".

Additionally, we suspect that the crimping pressure when sealing the cells is a potential source for inconsistencies between different sample series. The *CC-type_A*, *_B*, *_D* and *_E* were sealed with commercial crimping equipment (MSK-110, MTI corp.) and the pressures applied ranged from roughly 500 to 750 psi. The *CC-type_C* cells, on the other hand, were sealed with a deviating press (BTinnovations) at pressures ranging from 1100 to 1300 psi. This leads to a slight deformation of the outer edge of the coin cell housing, which may result in a better sealing and possibly lower cell resistances if the stack pressure was higher. Lastly, additional differences may originate from cell holders, testing temperature fluctuations and the accuracy of the battery cycler equipment. In the following we will elaborate on each of the above mentioned parameters.

Since *CC-type_C* showed the best performance and similar data to the benchmark pouch cells, cells of that type (*CC-type_C2*) were run using the RiDC test every 100 cycles to check whether this procedure has an effect on the performance of the cells (note that also a rate test was performed for *CC-type_C2* before long-term cycling). From these cells also RiDC plots were made and compared to the areal inner resistances of the pouch benchmark cells (see Figures S3 and S9). The inner resistance of the coin cell is slightly higher and increases much more rapidly with cycling than that of the pouch cell.

Coin-cell steel grades

During the round robin study three labs assembled coin-type cells based on steel parts with grades SUS304 vs. SUS316L. The selection of steel grade SUS304 significantly worsened the test results compared to SUS316L. Within commercial coin cell parts common steel grades are SUS304, SUS316 and SUS316L. All of these steels contain considerable amounts of chrome and nickel but differ in molybdenum and carbon content (cf.

Table S1). As a result, the corrosion resistivity varies and increases accordingly in the order of SUS304 < SUS316 < SUS316L. Exemplarily, *CC-type_A* series data is shown (Figure 7), where cell tests using coin cell parts of SUS304 (*CC-type_A2*) and SUS316L (*CC-type_A*) stainless steels were conducted to emphasize on the difference of cell KPIs for differently corrosion resistant coin cell parts. Average values for both data series during the formation cycles are given in Table 5. For all samples in the test series, coin cells built from SUS316L steel clearly showed notably higher absolute capacities on average as well as significantly improved capacity retentions of over 1500 cycles before the 80% relative capacity limit was reached.

Based on the cycling results it is reasonable to conclude, that less corrosion resistant SUS304 stainless steel, leads to parasitic and lithium consuming side reactions at high potentials, which significantly reduce the cycling performance of full-cells. The impact of parasitic reactions is quantified by the initial coulombic efficiencies (CE) in Table 5. Coin cells from SUS304 steel show on average a 4.5% lower CE on the first cycle compared SUS316L steel. The former reached only values of about 98% after four formation cycles, whereas with cells from SUS316L steel an average CE of 98.6% is obtained already
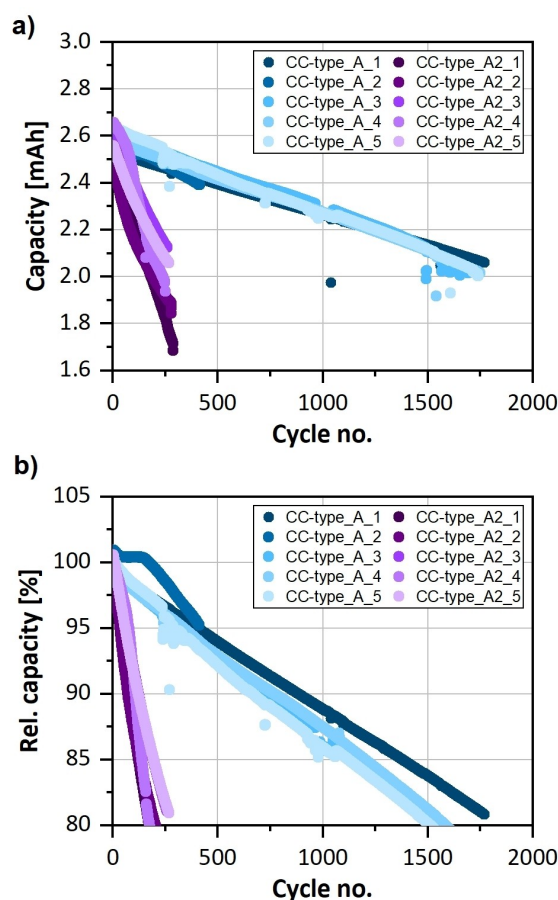
Figure 7. a) Absolute and b) relative long-term capacity decay upon 1 C charge/ discharge vs. cycle number for identically built cells with SUS316L (blue) and SUS304 (magenta) stainless steel coin cell casings.

Table 5. Charge and discharge capacities and CEs during cell formation, for identically built coin cells using CC-type_A (steel grade SUS316L, 5 cell average) and CC-type_A2 (steel grade SUS304, 4 cell average).

| Steel grade	SUS316L stainless steel			SUS304 stainless steel		
Formation cycle		Avg. capacity	Avg. Coulombic efficiency		Avg. capacity	Avg. Coulombic Efficiency
	Charge [mAh]	Discharge [mAh]	[%]	Charge [mAh]	Discharge [mAh]	[%]
1	3.27(4)	2.80(5)	88.5(5)	3.29(4)	2.77(6)	84.0(8)
2	2.81(5)	2.77(5)	98.6(2)	2.85(4)	2.77(3)	97.3(6)
3	2.78(5)	2.76(5)	99.1(2)	2.80(3)	2.74(4)	97.7(4)
4	2.76(5)	2.74(5)	99.3(1)	2.76(4)	2.70(5)	98.0(4)

on the second cycle and increased further to 99.3% after four formation cycles.

Interestingly, it was also found that the differences in the coin cell steel appear to affect the cell resistance from RiDC measurements as well. For the data series *CC-type_E* (SUS316L) and *CC-type _E2* (SUS304) RiDC measurements were carried out after formation and after 100 cycles (RiDCs at SOC30 are depicted in Figures 8b and S5). The SUS304 steel parts cause a greater overall cell resistance of $69 \pm 9\,\Omega\,cm^2$ compared to the SUS316L steel parts with only $51 \pm 6\,\Omega\,cm^2$. This difference is substantial and a potential hindrance for the comparability of cycling results from different labs. Moreover, higher cell resistances can affect rate capability tests adversely, as can be seen in Figure 8(a) (mean values and error bars from standard deviation determined from five individual cells each). Coin cells based on SUS304 steel (*CC-type_E2*) deviate as early as 1 C (~ 2%) from the best performing coin cell, culminating in a maximum capacity difference of ca. 20% at highest C-rate 5 C. Overall, the best performing coin cell delivers 15% less capacity at a discharge rate of 5 C compared to *LPC-5*. A thermal effect, which would lower the internal cell resistance of *LPC-5* cells and thus increase rate capability can be excluded here, as no significant heating (increase of temperature by 0.5 °C) was measured at 5 C discharge rate on the surface of *LPC-5_1*. In addition, *CC-type_E2* shows signs of aging after the rate-tests, which could be an indication of detrimental effects from corrosion processes.

As we have not carried out rate-capability tests and RiDC measurements for all sample series the results in Figure 8 should be regarded as a preliminary finding that probably should deserve more attention. Because of the varying resistances of the two cells build from different steel types, it stands to reason that even in the absence of corrosion processes rate-capability tests might yield ambiguous results depending which coin-cell type is used.

The findings, however, highlight that steel grade becomes a crucial parameter when full-cells with carbon-based anodes are investigated and high steel grades such as SUS316L are strongly advisable. It needs to be pointed out that it has already been shown that aluminum-coated coin cell housings can likewise positively influence the cell test results.[31] Although the impact on half-cell setups was not investigated, it is clear from an electrochemical standpoint that if the corrosion potentials of the coin cell steel are exceeded, parasitic reactions occur in cathode half-cells and full-cells alike and should be reflected in lower CEs (Table 5). In addition, degradation products of these parasitic reactions may induce a cascade of other adverse effects that deteriorate battery performance and cycle life.
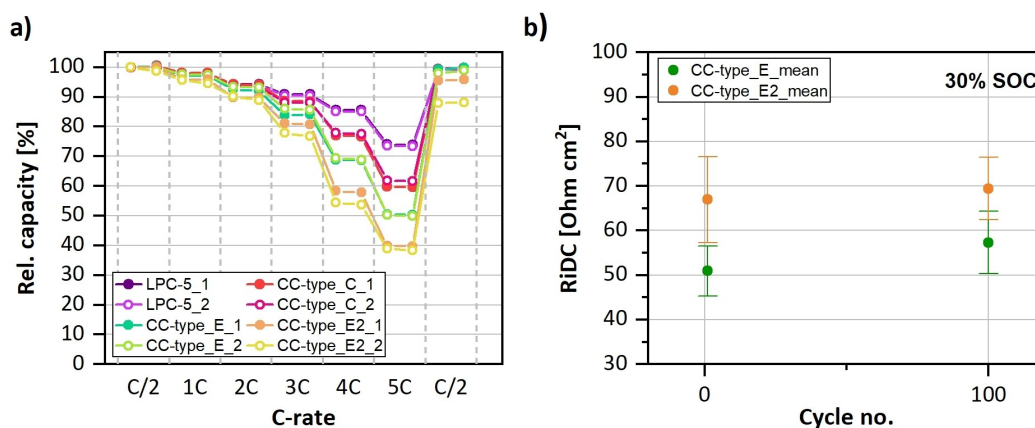
Figure 8. a) Rate capability of coin-type cells in comparison to pouch-type cells. Plot is showing relative capacities vs. C-rate for lab-size pouch-type cells vs. coin-type cells. b) Exemplary plot of RIDCs at SOC30 for 1st and 100th cycle after cell formation for coin-type cells, made of different steel types (CC-type_E: SUS316L, CC-type_E2: SUS304). Mean values and error bars from standard deviation were determined from five individual cells each.

Batteries & Supercaps

Research Article
doi.org/10.1002/batt.202300080

Chemistry Europe
European Chemical
Societies Publishing

Impact of testing equipment

The temperature and some aspects of battery testing hardware have been discussed in previous studies.[32] Herein, a brief discussion of the influence of cell connectors is complemented and, in addition to the standard testing environment described above, testing results from a reference setup are shown.

Even on a coin cell level, one prerequisite for good testing results is an appropriate cell contacting. Four-point contacting cell holders, or well-built two-point contacting cell holders, as shown in Figure 9(a and b), yield in uniform and reliable measurement results. For the latter, low resistances on the two wire path (R_w) are of utmost importance. In the case of the cell holder shown in Figure 9(b), R_w for instance is specified to < 5 mΩ by the manufacturer. Therefore, the voltage measured by the testing equipment corresponds very closely to the actual voltage of the battery. The wiring diagram of the four- and two-point contacting is shown in Figure S10. For the cell holder shown in Figure 9(b), a resistance of $R_w = 7$ mΩ was measured. For the cell holder shown in Figure 9(c) in contrast, combined cable and junction resistances summed up to 44, 48, 92 and 112 mΩ for four random channels. Corrosion at the junction between the ring connector and the screw led to high resistances on the two wire path and therefore can cause systematic errors in cell testing results. These values could be uniformly reduced to $R_w < 20$ mΩ for each channel by tightening the screws and therefore reducing the resistance between the screw and the cable lug. This example highlights that bad cell holder design can easily lead to additional resistances above 0.1 Ω in the series circuit shown in Figure S10(b). The effect of a resistance $R_w = 0.1$ Ω might be still negligible for high-impedance coin cells, where the internal resistance of the battery (R_i) for instance is 85 Ω, but becomes relevant for low-impedance coin cells (e.g., $R_i \approx 29$ Ω) and would become highly relevant for small pouch cells, where $R_i \lesssim 1$ Ω. The derivation of these values can likewise be found in the Supporting Information. At a nominal voltage of 4.000 V, for the aforementioned cells ($R_i = 85, 29$ and 1 Ω) the actual cell voltage would be reduced to 3.995 V, 3.986 V and 3.636 V, respectively. At least the last value is problematic at the very least, and would lead to a substantial falsification of the measurement results by premature shut-off in cycling reaching allegedly voltage limits. It should also be noted that the springs of cell holders might weaken after a period of time, which will result in differences in contact resistance. Further, contacts should be cleaned periodically to remove surface deposits.

A systematic investigation of the individual influence of different battery testers, cell holders and climatization is beyond the scope of this work due to the enormous effort involved in moving testing equipment into different buildings across our campus. Nevertheless, in order to demonstrate the impact of different testing conditions on the data quality and cycling results, 20 coin cells were built in the same manner by the same user. A total of 10 cells were assembled using SUS304 (*CC-type_A2*) and another 10 were built from SUS316L (*CC-type_A*) steel cell parts, respectively (Table 4). All cells were split in sets of five and studied under two different testing conditions listed in Table 6 that are commonly encountered in battery laboratories.

Our standard equipment for testing single-layer electrode stack pouch cells (*LPC-1–LPC-5*) and coin cells is setup 1 comprising of a BaSyTec CTS-LAB battery cycler with a BT
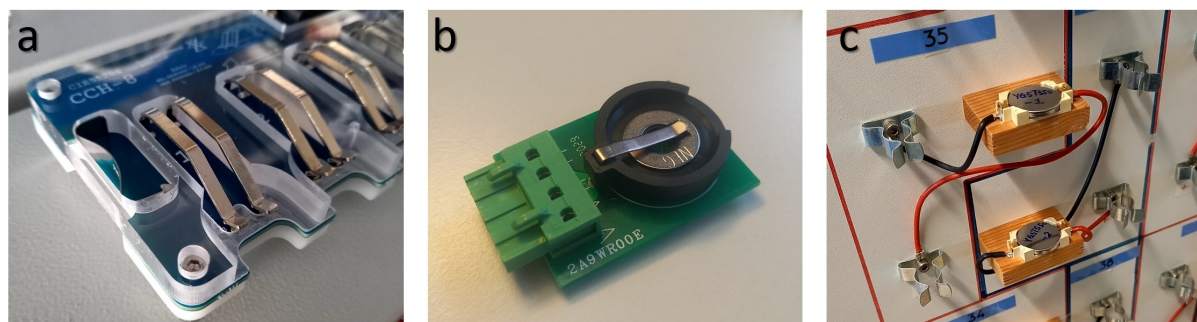
Figure 9. Different types of cell holders. a) Exemplary commercial four-point contacting cell holder. b) Exemplary commercial cell holder with short two point contacting distances and a resistance specified to $R_w < 5$ mΩ. c) Poorly designed homemade cell holder.

Table 6. Comparison of different testing environments and conditions. The standard testing conditions (cf. experimental section) yield significantly better and more reliable data than the reference testing conditions. The current ranges used for coin cell testing are in bold letters.

	Standard testing setup (setup 1)	Reference testing setup (setup 2)
Battery tester (BT)	Basytec CTS-LAB	Reference Testing station
BT current ranges	**1 mA, 15 mA**, 250 mA, 3 A	100 μA, **10 mA**, 1 A
BT current range overlap	6.6%, 6%, 8.3%	1%, 1%
Testing currents		309 μA (C/10), 3.09 mA (1 C)
Climatization	climate chamber (±0.1 °C)	climatized room (±1.5 °C)
Cell holder	commercial 2-point contacting cell holder ($R < 10$ mΩ)	homemade 2-point contacting cell holder (20 mΩ $\gtrsim R \gtrsim$ 200 mΩ)
Coin cell storage	rest over night at 40 °C before testing	immediate cycling after cell building

Batteries & Supercaps

Research Article
doi.org/10.1002/batt.202300080

Chemistry
Europe
European Chemical
Societies Publishing

current overlap in the relevant current range of around 6%. The cells are located in a climate chamber and connected to a commercial 2-point holder. In a different setup, setup 2, the current range overlap of the reference tester is notably smaller, the cell holder is homemade (as described above) and the cells are located in a climatized room with a temperature variation of up to $\pm 1.5\,°C$. The gap in current range between 100 µA and 10 mA of the reference battery cycler could give rise to more dispersion in the data points acquired during the formation cycle where the applied current is only 309 µA, i.e., 3.09% of the maximum current of 10 mA.

As a performance indicator for data quality and reproducibility the coulombic efficiency (CE) values over the first four (formation) cycles was compared between the different sample series, as shown in Figure 10 for the two test environments [a) setup 1 and b) setup 2] and the two steel types.

With the exception of a single cell which failed for unknown reasons, (*CC-type_A2_4*), the coin cells of both steel types tested in setup 1 yielded highly comparable results (Figures 7a and 10). The averaged capacities and CEs (SUS304: n=4

samples, SUS316L: n=5 samples) are provided in Table 5. On the other hand, within setup 2 larger fluctuations and considerable deviations in the CE on the formation cycles between different cells of the same series are obtained (Figure 10b). As can be readily seen from our example in Figure 10, reproducible data can be obtained using setup 1 independent of the coin cell steel, i.e., even in case of SUS304 steel. Clearly, acquisition of reproducible data with setup 2 is substantially more challenging.

For the sake of completeness, the long-term cycling data from cells operated on setup 2 are provided in Figure S11: As indicated by the formation cycles, long-term data collected by setup 2 yields in greater apparent capacity decay of the cells, and also much lower reproducibility of data obtained from 5 cells than setup 1.

It becomes obvious that high-quality and well-calibrated testing equipment in combination with climate chambers, appropriate cell contacting as well as the resting of the cells before the cell test, yields significantly better and more reproducible data of our graphite-NCM111 full-cells. However, it needs to be emphasized that the less consistent data set is by no means solely due to older battery tester, but rather a result of a combination of disadvantageous factors listed in Table 6.

Figure 10. a) Influence of the standard testing conditions vs. b) the reference testing conditions on the Coulombic efficiency measured during the formation cycles. Two sets of 10 identically built coin cells made of SUS316L stainless steel (blue, CC-type_A) and SUS304 stainless steel (magenta, CC-type_A2) were built.

Stack height and pressure

The height of the cell stack is another crucial parameter for valuable test results. Pouch-type cells have sufficient pressure on the electrode stack due to vacuum sealing and resulting atmospheric pressure on the stack ($\sim 10\ N/cm^2$). However, during aging with possible gas formation this stack pressure decreases. In contrast, when pouch cells are braced, stack pressure increases during cycling due to increase of the thickness of the electrode stack, for example continuous growth of SEI or lithium plating. The sealed housing of hard case coin cells compensates for atmospheric pressure effects from the outside and is mainly set by the cell building conditions. This means that the height of the stack components itself in combination with the spring force directly influence the pressure and contacting within the housing. An exact determination of the stack pressure is rather difficult in coin cells, but can be estimated, when the dimensions of the cell parts and the spring force are known. In Figure 11 a sketch of the coin cell setup with the cell stack and the space available inside a commercial CR2032 coin cell made from SUS316L steel are shown.

The minimum stack height for the CR2032 coin cell was determined to be 1.05 mm, calculated from the cell height (3.2 mm) subtracting the steel thickness of the lower and upper casing (2×0.25 mm), the thickness of the spring washer steel (0.25 mm) and the free height of the spring (1.4 mm). If the stack components (spacer, anode, separator, cathode) do not reach this minimum height of 1.05 mm, the insufficient height of the cell stack will result in either no reliable cell characterization or poor measurement data. Supporting Figure S8 shows
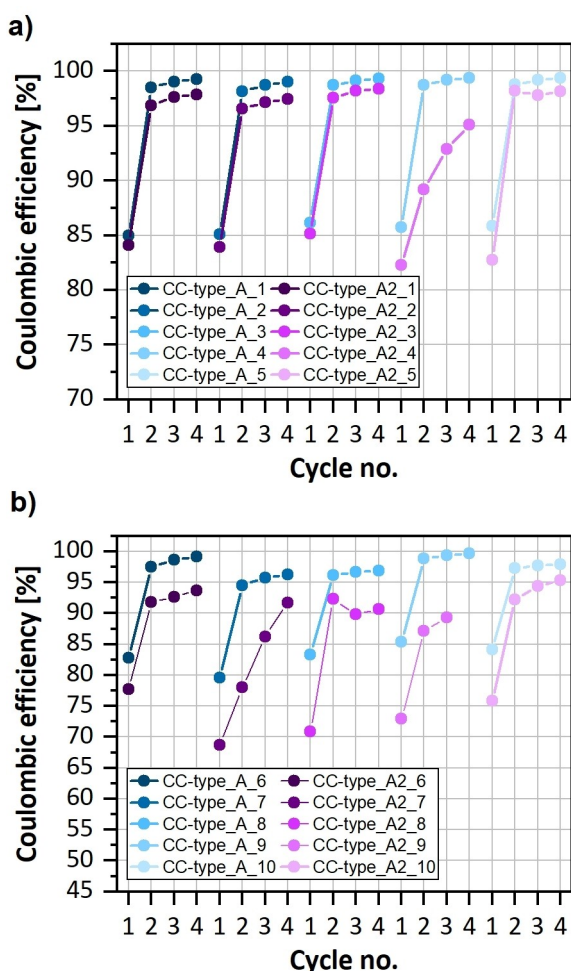
Cell stack

CR2032 Coin cell case
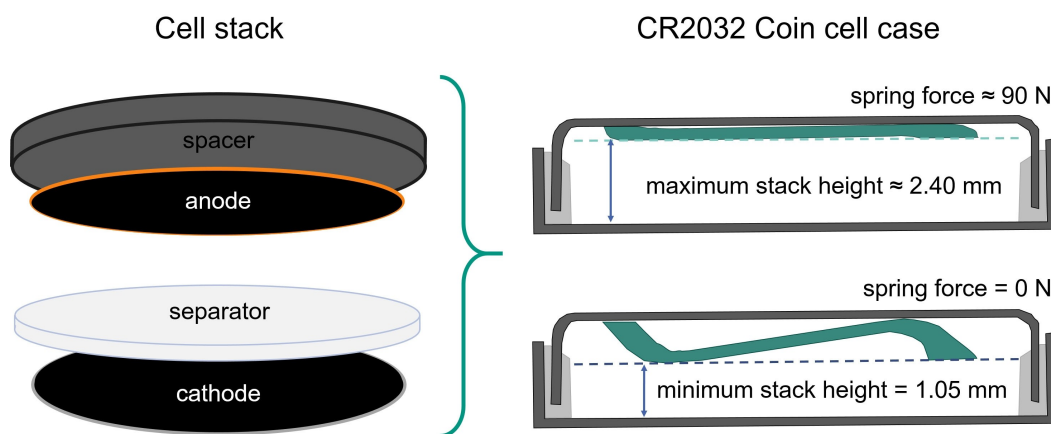
Figure 11. Schematic depiction of coin-type cell setup and height consideration for a CR2032 casing. The dimensions and spring force correspond to a commercially available cell case made of SUS316L stainless steel with at thickness of 0.25 mm.

a typical noisy voltage profile when the electric contact is insufficient, see also Table 4, *CC-type_D*. Since the voltage reading is incorrect, voltage limits might be reached too early because of additional contact resistances, thus resulting in apparent poor capacities. The maximum stack height is roughly 2.40 mm when the spring almost fully compresses to 0.3 mm. With a stack exceeding 2.40 mm, the cell may not close properly. In addition, given a spring force of approximately 70 N/mm the stack pressure for a stiff 2.4 mm stack would sum to roughly 90 N, which is comparatively high for a liquid electrolyte system. Based on the cathode and anode with a diameter of 16 mm and thus an area of ~2.0 cm², a spring compression of about 0.3 mm should yield desirable pressure of roughly 10.5 N/cm², which is comparable to one atmosphere (10.1 N/cm²) for a fully evacuated pouch bag cell.

In order to approach the corresponding stack heights, it is essential to be aware of the dimensions of the installed cell components. Depending on the application, cathodes on aluminium current collector foils often have a thickness of 0.05 to 0.18 mm, while graphite anodes are usually somewhat thinner (e.g. 0.03 to 0.05 mm). Lithium foil is typically available with thicknesses of 0.25 to 0.75 mm. A wide thickness range is likewise found for the separators. While polyolefin-based commercial separators are often 0.02 to 0.03 mm thick, glass fiber separators frequently used in coin cells have thicknesses of several hundreds of μm, for example 0.26 mm (Whatman GF/C) or 0.68 mm (Whatman GF/B), respectively. The metal spacers, which are necessary to transfer the spring force evenly to the cell stack, allow the stack height to be flexibly adjusted. They are commonly offered by manufacturers in thicknesses of 0.3, 0.5 and 1 mm. A list of the thicknesses of some cell components is given in Table S2.

To obtain reliable coin cells that work well based on these considerations and the cell tests shown in Figure 6, we strongly recommend knowing and complying with the minimum and maximum stacking heights (see Table 4 for stack and composition details on tested coin cells). In addition, it should be kept in mind that for high stacks (e.g. >2 mm) pressures of 70 N

and more can occur, which could possibly cause deviations from the behaviour of the same materials in pouch bag cells.

Other considerations for cell manufacturing

It was demonstrated above that a proper cell stack pressure, as well as the steel grade used within the cell casing have a great impact on electrochemical performance and its reproducibility, there are other factors to keep in mind when assembling battery cells, especially in coin-type configuration. For the sake of completeness, we would like to provide a brief overview of which other factors we have not touched upon, but are potential sources for poor reproducibility and/or comparativeness between various cell setups. Because of the numerous additional experiments, a full permutation of all potential parameters in the test matrix would require, aside from time and availability of test channels, only a qualitative discussion is provided in the following.

Firstly, the separator type (material, coating) and thickness as well as its tortuosity can influence the cell performance greatly. For one, the separator or coating material could be chemically incompatible with the electrolyte. For example, commonly used glass fiber separators are composed of SiO_2 which might react with traces of HF formed in the coin cell during operation. Improper drying of glass fiber separators can drag traces of water into the electrolyte, causing HF formation[33] in the first place. At the same time, SiO_2 may act as a HF scavenger but produces more H_2O and more electrolyte degradation in the process.[34] Additionally, even within the class of glass fiber separators, there are differences in the SiO_2 content so that two given glass fiber separators might not provide directly comparable cell test results. Recently, it has been found that PET containing tape (here we uses a PET-based separator) within cells can form redox shuttle molecules, namely DMT, which cause self-discharge of the cell.[35] This effect, however, can be negated using VC as an additive, which is the case in the present study. The thickness of the separator and also its porosity and compressibility will directly influence

Batteries & Supercaps

Research Article
doi.org/10.1002/batt.202300080

Chemistry
Europe
European Chemical
Societies Publishing

the stack height and thus the cell pressure. Secondly, the absolute amount of electrolyte, in particular when additives are used, plays a major role for cycle life. It is also the factor varied the most in academic and/or R&D cell assembly. Using excess electrolyte masks drying up and degradation processes and thus artificially extends the cell's lifetime. A frequently discussed example is the use of fluoroethylene carbonate (FEC) in graphite-silicon or silicon electrodes. In these systems, complete consumption of FEC is marked by a distinct drop in capacity retention.[27,36,37] However, from a material testing perspective, excess electrolyte volumes "turn off" some of the undesired side reactions described above and therefore allow the investigation of other degradation phenomena.[38,39] Lastly, insufficient drying of cell components (electrodes, separators or coin cell parts) or high moisture levels within the electrolyte can lead to electrolyte and electrolyte salt decomposition reactions (e.g., electrolytes containing $LiPF_6$ as conducting salt), resulting in aging effects.

The value of rate capability tests in coin-cells

Lastly, we would like to return once more to the rate-capability tests conducted for both pouch- and coin-cells in this study. One of the major KPIs in battery research rate-capability is frequently equated with high fast charging capabilities on a device level. Our comparison in Figure 8(a) clearly highlighted that even the best performing coin-cell assemblies (*CC-type_C*) are not only far from any realistic and practical cell assembly, but also perform poorly compared to pouch cell assembles (*LPC-5*) although the electrodes originated from the same sheet.

The samples *CC-type_C* keep up with the pouch-cell performance up to C-rates of 2 C showing similar capacity retention. Starting from a rate of 3 C deviation of ~2% (for 4 C~8%, and 5 C~14%) are observed. *CC-type_E* with a different stack height still shows comparable results with the pouch-cell assembly and *CC-type_C* up to a C-rate of 2 C. Major deviations of ca. 15% in capacity drop are observed at 5 C with respect to the best coin cell results (*CC-type_C*).

The origins of differences between pouch and coin cells are manifold. For instance, the current densities of the rate-test, given in C-rates, refer to the areal capacity of the electrodes, i.e., pouch and coin cell setups experienced the same current density but different total currents. This factor is important to highlight, since lab-size pouch cells have smaller inner resistances (~45 Ω cm^2 @SOC30) compared to the coin-type cells (~55 Ω cm^2 @SOC30). Besides a larger electrode area and thus a lower electronic resistance, the welded contacts in pouch cells greatly decrease the electronic resistance at high total currents. In contrast, coin cells simply contact electrode and cell housing physically through the applied stack pressure. As a result, electrodes with high loadings tested in coin cells may suffer disproportionally from higher inner resistances and poorer contacts. In turn, statements about rate capability may carry little weight beyond moderate current rates (~1–2 C), at least when electrodes with meaningful areal capacities are

tested. Furthermore, it is worth noting that on a lab scale many electrodes are not calendered, which further aggravates the performance in a rate-capability test.

Conclusions

- Electrodes need to be densified for proper data acquisition of rate capability tests. However, for determination of the capacity at low C-rates up to C/2 (where 1 C = 1.75 mA/cm^2), reliable capacity data can be obtained for NMC111 and graphite-based electrodes even when electrodes are not calendered. The effect of calendering on rate-capability is much stronger on NMC-based cathodes than graphite-type anodes most likely due to the higher conductivity of graphite particles then NMC particles. On the other hand, for long-term cycling it is demonstrated that densification of both, the NMC cathode and the graphite anode plays a crucial role in achieving high capacity retention over multiple thousands of cycles. However, during ageing, calendering of the anode has an even greater effect on capacity retention than densification of the cathode.

- The reproducibility and data quality of coin cell tests is highly influenced by a number of factors: proper cell contacting, the temperature of the testing environment, suitable current ranges and calibration of the battery tester, and sufficient resting of the cells before the cell test to ensure wetting of the separator and the electrodes.

- The best full-cell Li-ion battery results were obtained when using coin cell parts made of SUS316L stainless steel with a stack height of 1.6 mm (cathode, separator, anode and spacer), QM-A glass fiber as separator and 110 μL electrolyte within a CR2032 format. Using SUS304 steel parts, systematically worse cell performance (rate-capability and long-term capacity retention) was achieved compared to when using SUS316L steel parts.

- Full-type coin cells have a great potential: they can show long-term performance nearly as good as pouch-type cells under proper conditions (drying of components, cell stack height and pressure, casing steel type, appropriate separator and its quality, proper crimping including proper sealing).

- Full-type coin cells have their limits: typically the electrolyte to active material ratio is too high which skews practical performance compared to large format cells. Also, no thermal effects are depicted in coin-cells and with that thermal degradation effects are masked. Additionally, the rate capability measured is underestimated as the higher resistance of the coin cell itself falsifies true capability of the electrodes.

- Half-type coin cells skew the capacity data due to the endless reservoir of lithium. Their long-term performance, especially with the use of glass fiber separator, is also limited due to the dendritic plating phenomenon of lithium leading to cell failure after only ~100–200 cycles depending on the amount of electrolyte used and also the amount of stripped/plated lithium per cycle.

Experimental

KIT-BATEC pouch cell assembly

Cell assembly of the small laboratory-size pouch cells (*LPC*) and large multi-layer pouch cell (*9 Ah*) was carried out within a dry room (−68 °C dew point) at the semi-automated manufacturing line with commercially available electrodes at the Battery Technology Center at Karlsruhe Institute of Technology (KIT-BATEC). The anodes, which consist of graphite, are 5.2 cm × 5.2 cm in size for the lab-size cell, and 13.9 cm × 21.2 cm for the large format. Cathodes consist of NMC111 and are 5.0 cm × 5.0 cm in size for the lab-size cell and 13.5 cm × 20.8 cm for the large cell. The separator used is a commercial ceramic coated polyethylene terephthalate fabric (CC-PET) and 5.5 cm × 5.5 cm in size for the lab-size cell, and 14.3 cm × 21.6 cm for the large cell. Electrodes and separators were dried under reduced pressure for 24 h at 130 °C and 180 °C, respectively, before assembly of the cell stack. The lab-size cells contain either one single-sided coated cathode and one single-sided coated anode or double-sided coated electrodes separated by one sheet of separator. In contrast, large cells contain only double-sided coated electrodes and the stack includes nine cathodes and ten anodes. The lab-size cells were filled with 450 μL (single-sided coated electrodes) or 700 μL (double-sided coated electrodes) while large cells were filled with 35 mL electrolyte containing 1 M $LiPF_6$ in 50/50 (w/w) ethylene carbonate (EC) and dimethyl carbonate (DMC) with 3 wt.% of vinylene carbonate (VC) as an additive (already mixed, purchased from Gotion). After filling, the cells were sealed under reduced pressure. Subsequently, the cells were stored over night at 40 °C for sufficient wetting of the separator and electrodes. The large format *9 Ah* cells were evacuated after formation prior to long-term cycling.

Coin cell assembly

Coin cell assembly was performed in different laboratories within argon-filled gloveboxes using the same electrode materials, the same drying procedure and the same electrolyte as for pouch cell assembly. The electrolyte was filled in small dried aluminium bottles and taken from a large bottle (batch). Commercial coin cell components of either steel grades SUS304 and SUS316L (in each case with equal steel grade for a set of components including housing and spacer) and polypropylene sealing gaskets were used. For full-cell assembly, the size of the cathode was either 14 or 15 mm in diameter, whereas the anode size was 16 mm in diameter. In half-cell configuration Li chips from MTI Corporation (15.8 mm in diameter, thickness of 250 μm), against graphite/NMC111 with diameters of 14 mm were used. Metal spacer thickness (0.5 and 1 mm) and the separator were varied in round robin tests using either glass fiber GF/B, GF/C or QM-A (Whatman) or the CC-PET separator mentioned above. The electrolyte volume likewise varied from 110–350 μL. Before electrochemical measurements, the cells were stored at 40 °C over-night for sufficient wetting, if not stated differently.

Electrochemical data acquisition

The small pouch cells and coin cells were tested with BaSyTec CTS LAB instruments. Additionally, for demonstration purposes, a reference testing rig was used, a detailed description of which will be given in Section "Impact of Testing Equipment". The cells were stored in climate chambers at 25 °C (± 0.1 °C), except for coin cells of *CC-Type_C* which were cycled within a climatized room of 25 °C (± 2 °C). The *9 Ah* pouch cells were tested with a BaSyTec XCTS 50 A system, and cells placed in a climatized room of 25 °C (± 2 °C).

For all pouch cells a four-point contacting was realized. The single-sided coated cathodes have a practical capacity of 1.75 mAh/cm², so that 1 C was defined as 1.75 mA/cm² for all cell formats. Single-sided anodes had a capacity of 2.10 mAh/cm² at 1 C. For the formation step four cycles were applied, where charging was performed with constant current (CC) at C/10 until a voltage of 4.2 V was reached with subsequent charging at constant voltage (CV) until the current dropped below C/20. The discharge was performed using CC of C/10. Finally, the cells where charged to 3.7 V using C/10 CC for storage until the next cell test was performed. An asymmetric rate test was performed on half- and full-cells, meaning that charging was performed with a C-rate of C/2 CC with a CV phase (at 4.2 V for full-cells; 4.3 V for cathode half-cells; 0.005 V for anode half-cells) (until $I < C/20$) and rates in discharge direction were varied from C/2 to 5 C until a cut-off voltage of 3.0 V for full-cells and cathode half-cells, and 1 V for anode half-cells. To check for degradation due to the rate testing C/2 discharge was included at the end of the test procedure. For each C-rate two full cycles were applied. For long term cycling, all cells were cycled applying 1 C CC with CV until $I < C/20$ and 1 C CC discharge current. The voltage window for full-cells was 3.0–4.2 V, cathode half-cells 3.0–4.3 V, and anode half-cells 0.005–1 V. Some cells were long-term cycled using a "check-up cycle" every 100 cycles: measurements were made at five states of charge (SOCs), namely 10%, 30%, 50%, 70% and 90%, based on the determined cell capacity just before the test. For all SOCs direct current internal resistances (RiDC) were determined by use of current pulses of 1 C in discharge direction for 20 s. Applying Ohm's law, the DC internal resistances were determined using the potential drop (difference between the potential at the end of the pulse and the potential in rest state before the pulse) and the applied current for the respective pulses.

Further characterization

Cross sections of the electrodes were prepared by ion-milling using argon-ions (TIC-3X, Leica Microsystems). The electrodes then were studied by scanning electron microscopy (SEM) with a Zeiss Supra 55 FE-SEM using an acceleration voltage of 5 kV. To determine the loadings of the electrodes, discs and adjacent uncoated pieces of the current collector foils (16 mm in diameter) were punched out and weighed. Based on the differences, the single sided mass loadings were determined. Cell holder wire and contact resistances were measured with a HIOKI BT3554 instrument.

Conflict of Interest

The authors declare no conflict of interest.

Data Availability Statement

The data that support the findings of this study are available from the corresponding author upon reasonable request.

[1] C. Zhang, F. Wang, J. Han, S. Bai, J. Tan, J. Liu, F. Li, *Small Struct.* **2021**, *2*, 2100009.
[2] P. Stüble, H. Geßwein, S. Indris, M. Müller, J. R. Binder, *J. Mater. Chem. A* **2022**, *10*, 9010–9024.
[3] A. Schmidt, A. Smith, H. Ehrenberg, *J. Power Sources* **2019**, *425*, 27–38.
[4] J. Zhu, Y. Wang, Y. Huang, R. Bhushan Gopaluni, Y. Cao, M. Heere, M. J. Mühlbauer, L. Mereacre, H. Dai, X. Liu, A. Senyshyn, X. Wei, M. Knapp, H. Ehrenberg, *Nat. Commun.* **2022**, *13*, 2261.
[5] J. T. Frith, M. J. Lacey, U. Ulissi, *Nat. Commun.* **2023**, *14*, 420.
[6] P. Johansson, S. Alvi, P. Ghorbanzade, M. Karlsmo, L. Loaiza, V. Thangavel, K. Westman, F. Årén, *Batteries & Supercaps* **2021**, *4*, 1785–1788.
[7] Y. Cao, M. Li, J. Lu, J. Liu, K. Amine, *Nat. Nanotechnol.* **2019**, *14*, 200–207.
[8] B. R. Long, S. G. Rinaldo, K. G. Gallagher, D. W. Dees, S. E. Trask, B. J. Polzin, A. N. Jansen, D. P. Abraham, I. Bloom, J. Bareño, J. R. Croy, *J. Electrochem. Soc.* **2016**, *163*, A2999–A3009.
[9] P.-M. Luc, S. Bauer, J. Kowal, *Energies* **2022**, *15*, 7949.
[10] F. J. Günter, C. Burgstaller, F. Konwitschny, G. Reinhart, *J. Electrochem. Soc.* **2019**, *166*, A1709–A1714.
[11] S. Chen, C. Niu, H. Lee, Q. Li, L. Yu, W. Xu, J.-G. Zhang, E. J. Dufek, M. S. Whittingham, S. Meng, J. Xiao, J. Liu, *Joule* **2019**, *3*, 1094–1105.
[12] V. Murray, D. S. Hall, J. R. Dahn, *J. Electrochem. Soc.* **2019**, *166*, A329–A333.
[13] G. Bridgewater, M. J. Capener, J. Brandon, M. J. Lain, M. Copley, E. Kendrick, *Batteries* **2021**, *7*, 38.
[14] F. Dai, M. Cai, *Commun. Mater.* **2022**, *3*, 64.
[15] D. R. Sørensen, M. Heere, A. Smith, C. Schwab, F. Sigel, M. R. V. Jørgensen, V. Baran, A. Schökel, M. Knapp, H. Ehrenberg, A. Senyshyn, *J. Electrochem. Soc.* **2022**, *169*, 030518.
[16] B. Gyenes, D. A. Stevens, V. L. Chevrier, J. R. Dahn, *J. Electrochem. Soc.* **2015**, *162*, A278–A283.
[17] J. Zahnow, T. Bernges, A. Wagner, N. Bohn, J. R. Binder, W. G. Zeier, M. T. Elm, J. Janek, *ACS Appl. Energ. Mater.* **2021**, *4*, 1335–1345.
[18] B. G. Westphal, N. Mainusch, C. Meyer, W. Haselrieder, M. Indrikova, P. Titscher, H. Bockholt, W. Viöl, A. Kwade, *J. Energy Storage* **2017**, *11*, 76–85.
[19] D. Mayer, A.-K. Wurba, B. Bold, J. Bernecker, A. Smith, J. Fleischer, *Processes* **2021**, *9*, 2009.
[20] J. Varela Barreras, *PhD Ser. Fac. Eng. Sci.* **2017**, Aalborg University.
[21] Y.-C. Chien, D. Brandell, M. J. Lacey, *Chem. Commun.* **2022**, *58*, 705–708.
[22] T. Nordh, R. Younesi, D. Brandell, K. Edström, *J. Power Sources* **2015**, *294*, 173–179.
[23] S. Malmgren, K. Ciosek, M. Hahlin, T. Gustafsson, M. Gorgoi, H. Rensmo, K. Edström, *Electrochim. Acta* **2013**, *97*, 23–32.
[24] F. Jeschull, J. Maibach, R. Félix, M. Wohlfahrt-Mehrens, K. Edström, M. Memm, D. Brandell, *ACS Appl. Energ. Mater.* **2018**, *1*, 5176–5188.
[25] S. Leroy, F. Blanchard, R. Dedryvère, H. Martinez, B. Carré, D. Lemordant, D. Gonbeau, *Surf. Interface Anal.* **2005**, *37*, 773–781.
[26] B. Liu, J.-G. Zhang, W. Xu, *Joule* **2018**, *2*, 833–845.
[27] R. Jung, M. Metzger, D. Haering, S. Solchenbach, C. Marino, N. Tsiouvaras, C. Stinner, H. A. Gasteiger, *J. Electrochem. Soc.* **2016**, *163*, A1705–A1716.
[28] E. Björklund, C. Xu, W. M. Dose, C. G. Sole, P. K. Thakur, T.-L. Lee, M. F. L. De Volder, C. P. Grey, R. S. Weatherup, *Chem. Mater.* **2022**, *34*, 2034–2048.
[29] T. Schott, J. L. Gómez-Cámer, C. Bünzli, P. Novák, S. Trabesinger, *J. Power Sources* **2017**, *343*, 142–147.
[30] V. Mereacre, P. Stüble, V. Trouillet, S. Ahmed, K. Volz, J. R. Binder, *Adv. Mater. Interfaces* **2023**, *10*, 2201324.
[31] X. Chen, W. Xu, J. Xiao, M. H. Engelhard, F. Ding, D. Mei, D. Hu, J. Zhang, J.-G. Zhang, *J. Power Sources* **2012**, *213*, 160–168.
[32] A. J. Smith, J. C. Burns, S. Trussler, J. R. Dahn, *J. Electrochem. Soc.* **2010**, *157*, A196.
[33] A. V. Plakhotnyk, L. Ernst, R. Schmutzler, *J. Fluorine Chem.* **2005**, *126*, 27–31.
[34] S. F. Lux, J. Chevalier, I. T. Lucas, R. Kostecki, *ECS Electrochem. Lett.* **2013**, *2*, A121–A123.
[35] S. Buechele, A. Adamson, A. Eldesoky, T. Boetticher, L. Hartmann, T. Boulanger, S. Azam, M. B. Johnson, T. Taskovic, E. Logan, M. Metzger, *J. Electrochem. Soc.* **2023**, *170*, 010511.
[36] D. Yoon, M. Marinaro, P. Axmann, M. Wohlfahrt-Mehrens, *J. Electrochem. Soc.* **2018**, *165*, A2467–A2469.
[37] Y. Surace, F. Jeschull, P. Novák, S. Trabesinger, *J. Electrochem. Soc.* **2023**, *170*, 020510.
[38] A. Ghamlouche, M. Müller, F. Jeschull, J. Maibach, *J. Electrochem. Soc.* **2022**, *169*, 020541.
[39] Y. Surace, F. Jeschull, T. Schott, S. Zürcher, M. E. Spahr, S. Trabesinger, *ACS Appl. Energ. Mater.* **2019**, *2*, 7364–7374.